CHEMISTRY OF MATERIALS

Article

Cite This: Chem. Mater. 2017, 29, 5886-5895

pubs.acs.org/cm

Electrochemical Interaction of Few-Layer Molybdenum Disulfide Composites vs Sodium: New Insights on the Reaction Mechanism

José R. González,*[,†,‡] Ricardo Alcántara,[‡] José L. Tirado,[‡] Alistair J. Fielding,*[,†,§] and Robert A. W. Dryfe*[,†]

[†]School of Chemistry, University of Manchester, Oxford Road, Manchester M13 9PL, United Kingdom

[‡]Laboratorio de Química Inorgánica, Universidad de Córdoba, Edifcio C3, Campus de Rabanales, 14014 Córdoba, Spain

[§]Photon Science Institute, University of Manchester, Oxford Road, Manchester M13 9PL, United Kingdom

Supporting Information

ABSTRACT: The direct observation of real time electrochemical processes is of great importance for fundamental research on battery materials. Here, we use electron paramagnetic resonance (EPR) spectroscopy to monitor the electrochemical reaction of sodium ions with few-layer MoS_2 and its composite with carbon nanotubes (CNTs), thereby uncovering new details of the reaction mechanism. We propose that the sodiation reaction takes place initially in structural defects at the MoS_2 surface that have been created during the synthetic process (ultrasonic exfoliation), leading to a decrease in the density of Mo^{5+} at low symmetry sites that can be related to the electrochemical irreversibility of the process. In the case of the few-layer MoS_2/CNTs composite, we found metallic-type conduction behavior for the electrons associated with the Mo paramagnetic centers and improved electrochemical reversibility. The reversible nature of the EPR spectra implies that adsorption/desorption of Na^+ ions occurs on the Mo^{5+} defects, or that they are neutralized during sodiation and subsequently created upon Na^+ extraction. These effects help us to understand the higher capacities obtained in the exfoliated samples, as the sum of electrosorption of ions and faradaic effects, and support the suggestion of a different reaction mechanism in the few-layer chalcogenide, which is not exclusively an insertion process.

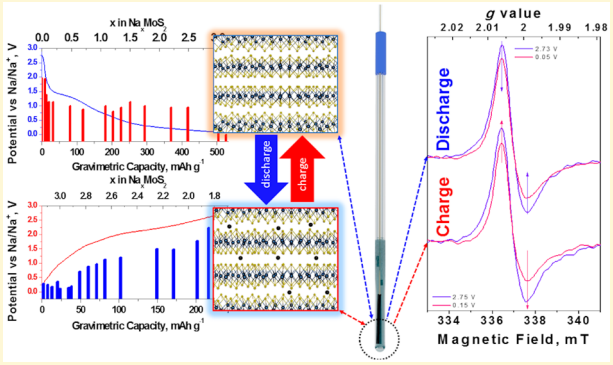

INTRODUCTION

The variety of issues that Li ion based energy storage technology faces[1,2] is promoting an increase in research for alternative technologies that may reach higher capacities and cycle stabilities with lower cost and "greener" chemistries. The high abundance of sodium in the Earth's crust, along with its high availability and low price, are pushing sodium-ion batteries as credible alternative candidates to lithium-ion batteries in the near future.[3−6] The similarities in both the chemistries of lithium and sodium with cathodic and anodic materials make imminent commercialization very appealing. Na, like Li, does not form a smooth film as it is electro-reduced during the battery charge process and favors the growth of dendrites upon cycling. These dendrites grow following the electric field lines eventually driving them to pierce the separator and to short-circuit the cell giving rise to possible ignition[1,7,8] of the low flashpoint organic solvents that compose the electrolyte. Therefore, there is a need to assemble batteries that avoid the use of pure Na metal. This leads to the necessity of developing materials that can intercalate, alloy, or undergo reversible reactions vs Na at a low enough potential for use as anode materials in a Na-ion battery. The development of such materials for scalable, safe, and economic Na-ion batteries is currently very challenging.[4] MoS_2 has been extensively studied as a host material for intercalant lithium ions and has been reported as a promising negative electrode material due to its high theoretical specific capacity and relatively low price.[9−13] The structural modification of MoS_2 from bulk to nanoparticulate and finally to nanoplatelets, nanosheets, or mono/few-layer 2D structures has been reported to improve the electrochemical behavior of the chalcogenide by increasing, first, the interlayer distances and subsequently the accessible surface and active sites where lithium can be accommodated.[12,13] It is important to note here that the similarities between the intercalation behavior of both Li^+ and Na^+ ions in different host materials might imply the same considerations for sodium as those conclusions obtained for lithium.[3,6]

The electrochemical intercalation of Na^+ into MoS_2 was observed by Park et al. by use of ex situ X-ray diffraction and transmission electron microscopy (TEM) measurements.[14]

Received: March 27, 2017
Revised: June 28, 2017
Published: June 28, 2017

DOI: 10.1021/acs.chemmater.7b01245
Chem. Mater. 2017, 29, 5886−5895

Electrochemical insertion of sodium ions in the MoS_2 layered structure was reported by Wang et al., who observed a structural transition modification through in situ TEM upon Na intercalation.[15] A nanospherical MoS_2/C composite has been synthesized and used as electroactive anodic material in Na batteries with high specific capacities (520 mAh/g at 1/10C).[16] David et al. used a paper-like composite of MoS_2 and graphene delivering a stable specific capacity of 230 mAh/g with outstanding efficiencies.[17] A hydrothermal synthesis route was used by Xie et al. to prepare a MoS_2/graphene composite as an anode material for Na-ion batteries.[18] Microparticulate MoS_2 in different shapes such as microflowers has been recently developed and its performance improved by using several types of binders.[19] All these methods use complicated synthetic routes that might not allow a profitable scale up of the electrode materials or its ready uptake by industry. It is well-known for graphene based materials (GBM) that the synthetic methods and the origin of the carbonaceous materials used as source materials, are crucial parameters for the final properties.[20] This might be extrapolated to the exfoliated compounds derived from transition metal chalcogenides and might explain the significant differences in the electrochemical performances obtained to the present day. Therefore, it is important to obtain a deeper understanding of the reaction mechanism taking place between few-layer MoS_2 and sodium ions in order to improve this promising material and make it an efficient and scalable negative electrode for real Na-ion batteries.

Electron paramagnetic resonance (EPR) spectroscopy is the ideal technique to characterize the existence of unpaired electrons,[21−23] giving rise to specific spectra (fingerprint-like) arising from radicals and ions from where quantitative, structural, and dynamic information can be inferred. Of specific relevance to this work is the sensitivity of EPR to study surface defects and the electronic properties of 2D materials.[23,24] There are few EPR studies on solid or few-layer MoS_2 with most studies focused on nanotubes. Silbernagel studied finely divided MoS_2 and MoS_3, and his findings showed the existence of two main types of EPR detected defects in the sulfides: sulfur coordinated (thio-Mo^{5+}) with g = 2.01 and oxygen coordinated (oxo-Mo^{5+}) with g = 1.91 and axial line shape.[25] Panich et al.[26] synthesized fullerene-like nanoparticles of MoS_2 and described the bulk 2H-MoS_2 (polytype notation for two layers for hexagonal unit cell) spectra as two overlapping signals: a broad line centered at ca. g = 2.3 assigned to paramagnetic impurities and a narrow and relatively weak asymmetric signal with g_{II} = 2.038(3) and $g_{\perp}$ = 2.0033(1) attributed to sulfur-coordinated defects (thio-Mo^{5+}). Their fullerene-like nanoparticles showed similar signals as well as additional signals with g = 1.98 and 1.97 which were assigned to other kinds of Mo^{5+} centered local defects that may be related to adsorbed species (O/OH) on the prismatic MoS_2 platelets.

Deroide et al.[27] studied the EPR lineshapes of amorphous or poorly crystalline molybdenum sulfides. They found resonances arising from Mo and S species. Paramagnetic sulfur signals at g = 2.027 could not be related to free sulfur chains in the sulfides, being more likely due to short chains stabilized by the local structure of the solid. Mo^{5+} was found in anisotropic sites, mainly due to local defects in the chain-like structure of amorphous sulfides (g_x = 1.927, g_y = 1.992, g_z = 2.024).

Young et al.[28] assessed the effect of a terminal sulfido ligand on the EPR spectrum of Mo^{5+} complexes, reporting a comparison to those effects of the oxo analogues. They observed that changes in g values and hyperfine constant values are dependent on the ligand type (oxygen or sulfur donor atoms) and on the position of the substituents. Their results demonstrate that a terminal sulfido ligand, which is bound to a Mo^{5+} center, produces lower g values than a terminal oxo ligand. At the same time, Hill et al.[29] found that the presence of disulfide interaction in Mo complexes reduces the g anisotropy of the EPR spectra compared to that of oxo-thio-Mo^{5+} complexes.

EPR in conjunction with electrochemistry has been used widely due to its selectivity concerning paramagnetic species.[30−32] During the electrochemical sodiation of few-layer MoS_2 samples, electron exchange reactions are expected as well as the partial reduction or oxidation of species that could imply the appearance of paramagnetic species detectable by EPR (i.e., reduction of the working electrode material during discharge, oxidation during charge). The possibility of recording these data with an in situ cell provides an excellent way of monitoring the changes in the electronic properties of the materials in real-time,[32−34] mainly in this case, the few-layer MoS_2. In this work, the EPR spectra of MoS_2 before and after exfoliation, as-prepared electrodes and during live galvanostatic cycling of in situ cells has been recorded and studied in order to understand the oxidation states and intrinsic or extrinsic defects created upon synthesis and during discharging-charging cycles of cells.

EXPERIMENTAL SECTION

Few-Layer MoS_2. The exfoliated molybdenum disulfide was obtained from bulk MoS_2 powder (Aldrich) with average particle size of 6 μm, following a procedure from our laboratory that has been described elsewhere.[35,36] The liquid exfoliation of the reactants yielded stable suspensions in *N*-methyl-2-pyrrolidone (NMP). Then, the suspension was dried under dynamic vacuum at 80 °C so that the solid could be recovered.

Few-Layer MoS_2/Carbon Nanotubes (CNTs) Composite. Powdered previously exfoliated MoS_2, Unidym HiPco SuperPurified (<5% wt % Fe catalyst) single wall carbon nanotubes (CNTs, supplied by Nanointegris, Boisbriand, Quebec, Canada) and powdered PVDF binder (Aldrich) were mixed in a weight ratio of 75:15:10 respectively, diluted in NMP and thoroughly sonicated in order to form a composite.

Working Electrodes. After ultrasonic stirring of the solids (few-layer MoS_2 or the mixture few-layer MoS_2 and CNTs in addition with 10% PVDF binder in both cases) in NMP suspensions, the obtained inks of the active materials were spread onto the surface of the platinum working electrodes and dried overnight at 80 °C under vacuum.

Electrolyte. The chosen electrolyte for the nonaqueous sodium cells was prepared by mixing ethylene carbonate (EC, 99% Aldrich) and diethyl carbonate (DEC, 99% Aldrich) in 1:1 volume ratio and then $NaPF_6$ salt was dissolved to a concentration of 1M.

Physical Characterization. X-ray diffraction (XRD) patterns were recorded with a Bruker D8 instrument with Cu$K\alpha$ radiation and reflection geometry. In order to obtain XRD patterns of recovered electrodes, the samples were protected from air and moisture with a cover of Kapton tape.

The morphology of the samples was characterized with scanning electron microscopy (SEM) by using an FEI Quanta 650 microscope, equipped with backscattered and secondary electron detectors. The discussion of the obtained data is included in the Supporting Information (SI).

The surface of the materials was studied by X-ray photoelectron spectroscopy (XPS). XPS spectra acquisition and imaging was performed on AXIS Nova instrument (Kratos Analytical Ltd., U.K.) and analyzed with CasaXPS software v.2.3 (Casa Software, Ltd.).

Continuous-wave (CW) EPR measurements were carried out on a Bruker EMX-Micro X-band spectrometer operating at a frequency of

DOI: 10.1021/acs.chemmater.7b01245
Chem. Mater. 2017, 29, 5886−5895

~9.6 GHz. Field frequency modulation, modulation amplitude, and microwave power were set to 100 kHz, 0.4 mT and 2.0 mW, respectively, in every case avoiding saturation effects. All the EPR spectra were recorded at room temperature. The obtained spectra were corrected using a strong pitch reference with a g value equal to 2.0028. The oxidation state for Mo in the studied MoS_2 was mainly Mo^{4+} with electronic configuration $4d^2$ but the samples can undergo partial reduction−oxidation during the synthetic route.[37] During the electrochemical cycling the subsequent redox reactions are also expected to cause changes of oxidation state with possible formation of Mo^{5+}, Mo^{3+}, Mo^{2+}, and Mo^0 ions, with electronic configurations $4d^1$, $4d^3$, $4d^4$, and $4d^6$, respectively. Configurations $4d^1$ and $4d^3$ are EPR active species due to their unpaired electrons. Owing to the interaction of the unpaired electrons with magnetic nuclei, the obtained spectra might present nuclear hyperfine interaction consisting mainly in splitting (hyperfine) of the resonances arising from the nonzero nuclear spin Mo isotopes: ^{95}Mo (15.9% $I = 5/2$) and ^{97}Mo (9.6% $I = 5/2$). For the electrochemical-EPR experiments, since the metallic sodium and electrolyte are highly reactive to air and moisture, the cells were assembled under an inert atmosphere. For this purpose the cell preparation was carried out inside a glovebox filled with argon with concentrations of O_2 and H_2O below 1 ppm. Finally, the cell was hermetically sealed by application of a thermoplastic film sealant tightly covering tube and wires. The reduced size of the in situ electrochemical cell, the small diameter of the EPR tube and wires, and the small volume of organic liquid electrolyte allow achievement of a high Quality factor (Q-value) during the measurements despite the possibility of nonresonant absorption. All the cells were left to relax for at least 1 h before measurements once they were connected to the potentiostat.

Electrochemistry. The electrochemical measurements consisting of galvanostatic cycling with set potential limits, during operando EPR were performed using a μAUTOLABIII/FRA2 electrochemical workstation. For comparison, electrochemical measurements of the same systems were tested in an AUTOLAB PGSTAT302N with a commercial electrochemical cell, to make sure that the electrochemical behavior of the materials in the in situ cell was free of artifacts arising from the EPR cell geometry. The electrodes used consisted of three platinum wires, insulated with PVDF, as current collectors. The wire's thicknesses differed according to their role. Reference (RE) and counter electrode (CE) wires were 0.1 mm diameter and the working electrode (WE) was 0.2 mm in diameter. The tip of the WE wire was not insulated and was mechanically flattened to give a foil-like electrode of 10 × 1 mm^2 so that the active material could be spread onto the surface as described in the materials section. A second insulated wire was placed parallel to the WE current collector wire in order to add robustness to the system. The counter and reference electrodes were made up by covering their noninsulated tips with Na metal. The wires were set up parallel to each other, and the tips were located vertically, placing the WE at the lowest part of the quartz tube. The RE and CE, were placed above the WE at a constant distance of 2 mm and 7 mm, respectively. The bottom of the test tube contained the material under study and was the only part which was introduced into the resonator avoiding any artifact signals arising from the rest of the cell components. The RE was placed as close to the WE as possible to minimize the effects of uncompensated resistance.

The XPS spectra obtained for bulk MoS_2 (Aldrich) (published elsewhere[36]) showed the presence of molybdenum and sulfur as well as adventitious carbon and oxygen. The Mo 4d energies were of typical values assigned to the 2H−MoS_2 phase as well as to Mo^{6+} related to the existence of oxidation of Mo in the surface oxide, MoO_3. Sulfur 2p binding energies were consistent with the existence of sulfur in two different oxidation states, most likely from the species S and S^{2-}. In the case of few-layer MoS_2 obtained following Coleman's liquid exfoliation method[35] and filtered through a microporous membrane, the 2H−MoS_2 phase was preserved but the intensity of the peaks related to Mo^{6+} was strongly diminished, suggesting that the exfoliation treatments removes the oxide present and hinders its formation. Sulfur binding energies were mainly found in agreement with the S^{2-} oxidation state for sulfur. The XPS results for the composite few-layer MoS_2/CNTs are discussed in the SI.

RESULTS AND DISCUSSION

CW EPR Preliminary Results. CW EPR spectra of the powdered pristine bulk (multilayer) and exfoliated (few-layer) MoS_2 samples were recorded at room temperature in order to observe the likely changes that the treatment could exert on the electronic structure of the chalcogenides. Figure 1 shows a very

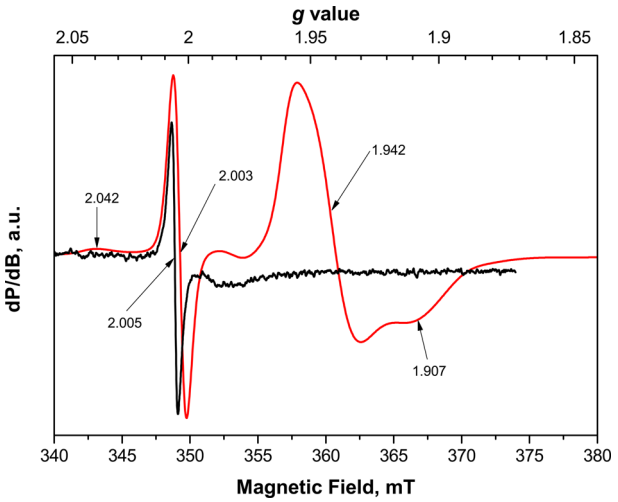

Figure 1. Mass-normalized EPR spectra of the (red line) exfoliated MoS_2 and (black line) bulk MoS_2.

significant change in the spectra after the exfoliation treatment of the MoS_2. Both signals are normalized in intensity in order to allow comparison of the line-shape. The difference in intensities of both spectra, normalized by weight of material, is on the order of 200 times greater (not shown) for the exfoliated samples, suggesting a much higher concentration of defects in the exfoliated sample.

The pristine material spectrum is composed, uniquely, by a relatively narrow asymmetric signal of characteristic g value at 2.005 that has been observed previously and ascribed to sulfur-coordinated defects (thio-Mo^{5+}).[26] These defects are most likely located (sulfur coordinated or sulfur and oxygen coordinated defects) at low symmetry sites and interstitial sulfur.[27,38,39] It is worth noting, here, that this signal can be considered as characteristic of the layered chalcogenide structures because of the lack of this signal in other nonfaceted morphologies such as MoS_2 nanotubes.[26,40−43]

In the case of the spectrum of the exfoliated sample, one can see that it consists of three different signals. A broad low intensity resonance at $g = 2.042$, a sharp and nearly symmetric resonance at $g = 2.003$, and a broad axial resonance with $g_\perp = 1.942$ and $g_{II} = 1.907$. Compared to the multilayer sample, the nearly symmetric line is slightly shifted to higher magnetic field in the region near the free electron (g_e) value and can be attributed to the same defects with slightly altered structure. The signal at $g = 2.042$ can be assigned to paramagnetic sulfur in short chains stabilized in the structure of the poorly crystalline MoS_2 in accordance with previously reported g values.[27,38,39,44]

The axial signal observed at higher magnetic fields that appeared after the exfoliation treatment possesses very close g values to those that have been previously reported for Mo^{5+}

DOI: 10.1021/acs.chemmater.7b01245
Chem. Mater. 2017, 29, 5886−5895

oxygenated species in amorphous or unsupported sulfides (g = 1.94 and 1.89)[38] and oxo-Mo^{5+} bonding in finely divided bulk chalcogenides (g = 1.91)[25] or attributed to Mo^{5+} atoms (g = 1.940, 1.924, 1.895) in environments with axial symmetry that could be promoted by lamellar structure.[39]

These values and assignments are in very good agreement with the expected changes in the chalcogenide upon the exfoliation treatment where a decrease in the particle size takes place and many Mo−S bonds can be destroyed causing unsaturated Mo atoms to form oxo-Mo^{5+} bonds. The assignment is further supported by the XPS results (Supporting Information) where the presence of Mo^{5+} was detected, and no quantifiable Mo^{3+} was observed. Moreover, Bruce Averill et al.[45] surveyed Mo^{3+} with S-donors, and found g values above and below 2, supporting the resonances interpretation as arising from Mo^{5+}.

In order to increase the electronic conductivity and mechanical stability of the 2H phase for a better electrochemical performance, the powder was mixed with super purified (<5% wt % Fe catalyst) carbon nanotubes (Unydim) and diluted in NMP. The resultant composite ink was spread on a nonconductive membrane and its EPR spectra were recorded. Not only do the CNTs increase electronic conductivity but they can also physically prevent the restacking of the few-layer MoS_2 and agglomeration of nanoparticles.[46,47] In Figure 2, the intensity-normalized EPR spectra of the exfoliated MoS_2/CNTs composite, and the CNT starting material, are shown. Several measurements were carried out in different orientations by rotation of the EPR tube, and no notable changes were found. In the composite spectrum one can clearly observe resonances at similar spectral positions as exfoliated MoS_2 with a signal at g = 2.0049 and a weak signal at g = 1.9822. This weak signal can be related to the shoulder observed in the few-layer MoS_2 spectra at similar g value from which no clear information can be inferred. No evidence of the resonance attributed to oxo-Mo^{5+} defects or restacking faults can be observed in the composite spectra.

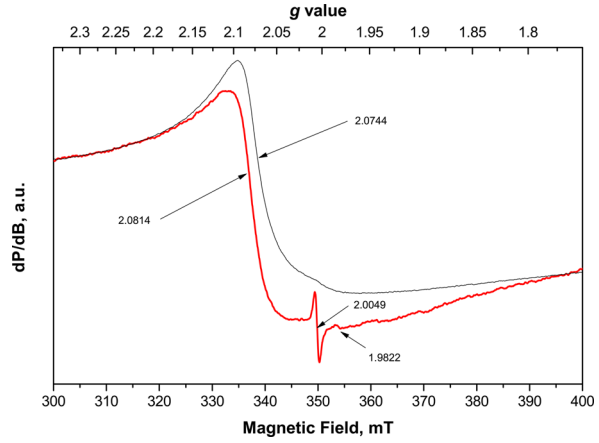

Figure 2. Normalized room temperature EPR spectra of the exfoliated MoS_2−CNTs composite (red line) on a nonconductive membrane and the bare carbon nanotubes (black line).

The super purified CNTs signal at g = 2.0744 shows a Dysonian-like line shape as expected for highly conductive carbon nanotubes, originating from electrons delocalized over the conducting domains of nanotube walls.[48] This signal shape is almost identical to that previously reported by Adhikari et al.[49] for neon irradiated carbon nanotubes and explained as arising from the deconvolution of four components, two located at extreme g values (g < 1.75 and g > 2.25) and the others in the g = 2.0 region. Those in the vicinities of g_e are related to either amorphous carbon or conductive delocalized electrons. The conductivity is observed to increase with the irradiative creation of defects, and the line shape evolves agreeing well with the measured spectra in Figure 2. It is worth noting that divacancy defects originating upon irradiation possess an electron spin state of S = 1 and produce an EPR signal at g = 4.0,[49] and these have been also observed in our sample (SI Figure S2).

In Situ/In Operando Electrochemical Measurements. A 4 mm quartz EPR tube was used as the case to assemble the cell. Figure 3 shows a schematic of the three-electrode configuration used in the measurements, discussed in detail in the Experimental Section. One important point to notice is the positioning of the counter and reference electrodes away from the region introduced into the resonator so that no counter-generated products could affect the obtained spectra.[31,33] The wires were placed inside the quartz tube, dipping their tips in 0.25 cm^3 of electrolyte, previously, added.

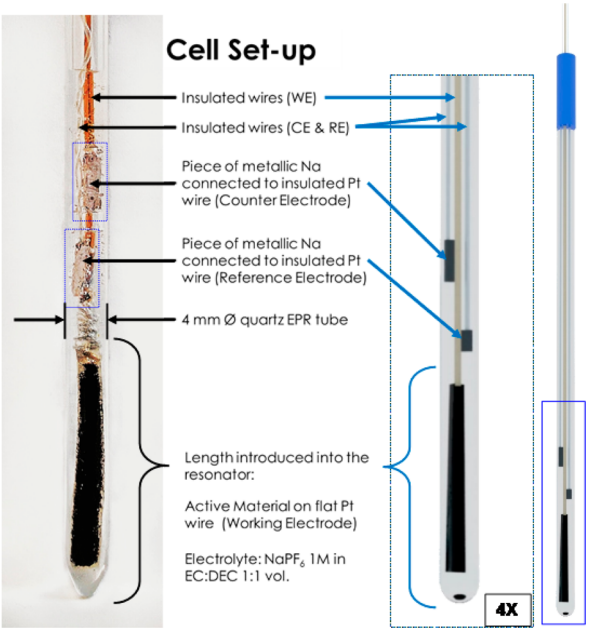

Figure 3. Picture (left) and schematic (right) of the utilized in situ electrochemical cell.

The in operando EPR spectra were collected at several steps during the electrochemical cycling allowing a real-time observation of signal evolution. In order to avoid parasitic chemical reactions taking place inside the test cell that could cause changes in the recorded spectra and lead to erroneous interpretation of them, time dependent measurements were carried out. No evidence of important changes in the spectra was found (see SI Figure S3). It should be stressed that the in situ EPR electrochemical cell, compared to those previously reported for batteries,[34] was made from widely available and fairly inexpensive materials as well as being of a very simple design, which allows it to be used to study active battery materials with relative ease.

It is known that upon discharge on first cycle of half cells, organic electrolytes generally decompose forming the so-called

DOI: 10.1021/acs.chemmater.7b01245
Chem. Mater. 2017, 29, 5886−5895

solid electrolyte interface (SEI). In the case of MoS_2, it is accepted that this interface is usually formed below 0.8 V vs Na/Na^+.[17] In spite of the formation of the SEI layer generally taking place during the first discharge (depending on the potential window and electrolyte used), the analytic comparison of the first cycles of both different materials in the same electrolyte and conditions vs metallic Na anode provides information on the very first reactions that take place between the active material and the charge carriers (Na^+) and can show the main differences in electrochemical behavior as well as the difference in reversible sodium extraction which is our aim herein. Both reversible capacities (amount of Na^+ extracted at the end of the first charge in both half cells) are influenced by SEI formation which will be different in the few-layer MoS_2 compared to its composite with CNTs because of their different morphology and conductivity.

It is worth noting here that the very low intensity of the EPR spectra generated by radicals in different organic electrolyte solvents does not allow their clear measurement at room temperature and obliges the measurements to be carried out at low temperatures. This would interfere with the correct electrochemical behavior of the cell by decreasing the Na^+ mobility.[50] Hence, the electrochemistry was analyzed under suitable conditions of temperature (RT) and no important contribution of those radicals could be inferred from the in operando spectra and, therefore, the signals arising are most probably exclusively due to the solid-state defects and/or paramagnetic ions referred to in the Introduction. In the case of the additive, poly(vinyl difluoridene) powder (Aldrich), used as binder, it gave no EPR signal, which is consistent with previous results obtained by others.[51,52]

Galvanostatic cycling and EPR spectroscopy of electrodes composed of few-layer MoS_2 (Ex-MoS_2), composite few-layer MoS_2 with carbon nanotubes (Ex-MoS_2/CNTs), and multilayer MoS_2 with carbon nanotubes (ML-MoS_2/CNTs) were carried out vs Na.

Electrochemical Properties of MoS_2. Some mechanistic hypotheses for the electrochemical sodiation of chalcogenides have previously been proposed. More precisely, the multilayer MoS_2 sodiation reaction has been proposed and described[14,15,17] as a phase transition during Na insertion from the 2H phase to the trigonal 1T when the number of Na atoms per formula unit is in the range 0.5 to around 1.1. These reactions generally take place in the range 2.6 to 0.4 V vs Na/Na^+. The further sodiation mechanism is described as a conversion reaction where 1T-$NaMoS_2$ can be partially transformed into nanoparticulate Mo(0) embedded in a Na_2S matrix. The sodiation reaction up to $x \approx 1.0$ has been determined to be nearly reversible (since it creates some distortion in the structure)[14,53] unlike the conversion reaction on further sodiation[14,15,54] due to microstrains that yield crystal structure distortions.

In general, the overall reaction can be described in the following insertion process:[17]

$$MoS_2 + xNa^+ + xe^- \rightarrow Na_xMoS_2 (x < 1) \quad (1)$$

and conversion reaction:

$$Na_xMoS_2 + (4 - x)Na^+ + (4 - x)e^- \rightarrow 2Na_2S + Mo \quad (2)$$

In the case of monolayer MoS_2, it has been theorized that a stable adsorption of Na up to Na_2MoS_2 (i.e., twice the amount of active sites for Na accommodation than in the multilayer samples) occurs, doubling the charge capacity of the material (theoretical capacity for monolayer MoS_2 = 335 mAh/g) throughout the mentioned potential window and yielding a diffusion for Na^+ 10^9 times faster at room temperature than that of the multilayer MoS_2.[55] However, the suggested more extensive breaking of Mo−S bonds induced by sodium intercalation above x = 1.0 can still be an important drawback, even when there are more available adsorption sites.[53] The capacity values obtained for the few-layer MoS_2 in conventional configurations (i.e., Swagelok type cell) in Figure S4 are consistent with an increased capacity compared to the multilayer chalcogenide agreeing well with expectations for few-layer MoS_2 (first discharge capacity at 0.85 V versus Na/Na^+ reached a capacity value of around 300 mAh/g that is a value of x in Na_xMoS_2 of around 1.8). However, the reversible capacity on the first cycle is only around 30%, which is consistent with previously reported electrochemical behavior when using that cutoff potential value due to the aforementioned structural changes, even though the material has been previously exfoliated.

Nanostructuring of MoS_2 can help to increase the miscibility of both phases upon sodiation due to the very short diffusion distances for the Na ions. As a result, the galvanostatic curves of few-layer MoS_2 do not show several extended plateaus, showing sloping curves instead.[54,56] In this case, however, the potential at which the first pseudoplateau takes place during discharge is higher than that reported for the multilayer MoS_2, and this may be due to the higher diffusion of Na for few-layer MoS_2 and lower diffusion barrier energies.[55] The few-layer MoS_2 in operando EPR measurements showed irreversible changes and are discussed in the SI (Figures S5, S6, and S7). In order to avoid this nonreversible behavior and for the sake of comparison, the experiment was also carried out with a composite made up of exfoliated MoS_2 and carbon nanotubes.

Electrochemical Properties of Few-Layer MoS_2/CNTs Composite. Figure 4 shows the EPR spectra of in operando Ex-MoS_2/CNTs composite electrochemical cell and the obtained galvanostatic curves for the first cycle of the composite against sodium as well as the g = 2.001 EPR signal intensity (obtained by double integration) for the measured potential steps. The EPR spectra are composed of a strongly asymmetric signal centered at g = 2.001 that can be explained as arising from $S-Mo^{5+}$ defects and a very weak and poorly defined signal at g = 1.954 attributed to oxo-Mo^{5+} and stacking defects.[27] In this case, however, in contrast to Figure 2, the more intense EPR signal shows a slight shift to higher magnetic field that can be attributed to a change of spin−orbit coupling derived from direct contact of the composite with the platinum foil current collector electrons in contrast with the signal of Figure 2 where the sample was powdered and without any current collector. This resonance shows a very strong asymmetry since the amplitude of the positive part of the signal is much higher than that of the negative (see SI Figure S8 for magnification). The asymmetry produces a clear Dysonian line shape and is directly related to the nature of the increased conductivity of the material and its effective grain size[57] compared to the pure few-layer MoS_2. This change can be related to the interaction with the CNTs that prevent restacking and agglomeration, which is consistent with the lower intensity and poorly defined signal at g = 1.954, related to these defects, suggesting that the addition of CNTs decreases the restacking faults. In the range from open circuit voltage to 1.47 V vs Na/Na^+ range (Figure 4, D) there is a strong decrease in the signal intensity at g = 2.001 that

DOI: 10.1021/acs.chemmater.7b01245
Chem. Mater. 2017, 29, 5886−5895

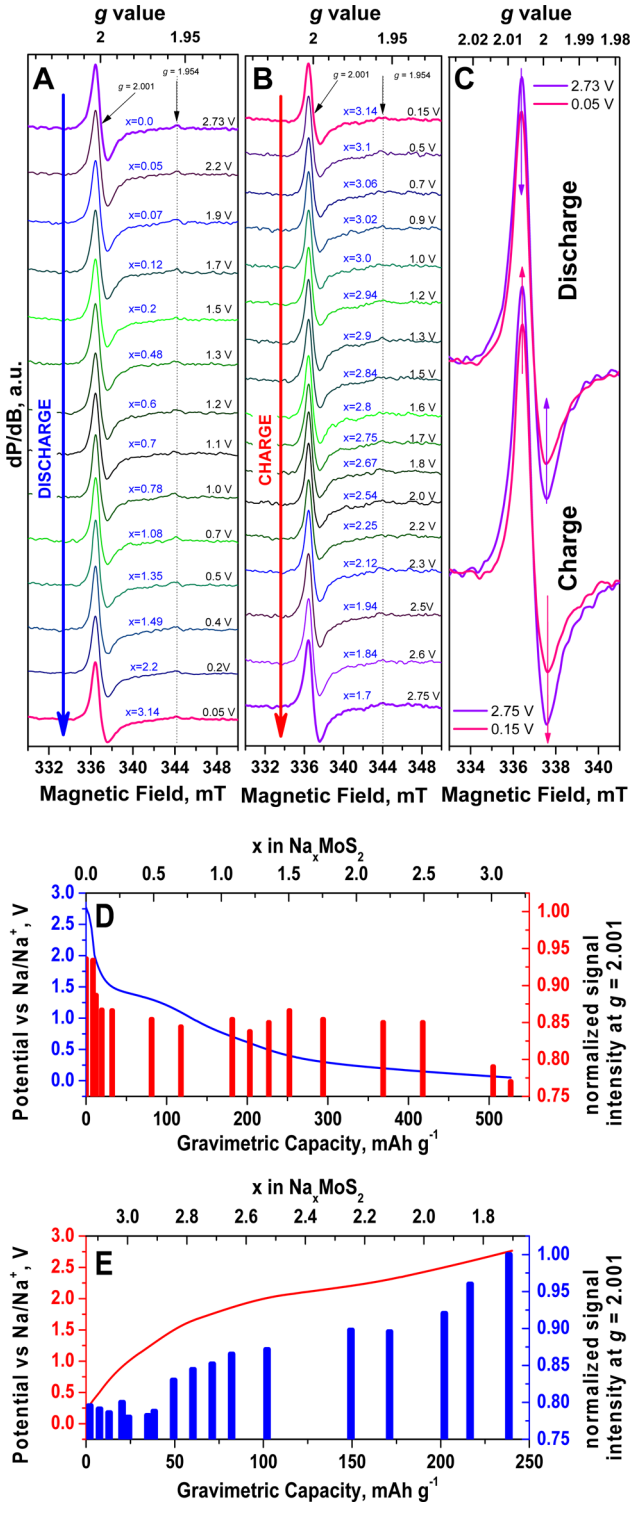

Figure 4. (A) In operando EPR spectra of few-layer MoS_2/CNTs composite for discharge obtained upon the battery cycling. (B) as of (A) for charge. (C) Maximization of first and last discharge and charge spectra in order to facilitate the observation of the undergone changes in the resonance lines. (D) Galvanostatic cycling profile of discharge of in situ Ex-MoS_2/CNTs composite cell versus Na. Normalized EPR signal intensity at g = 2.001. (E) as of (D) for charge.

coincides with the initial potential drop. During this range of potential the material sodiation has barely started, and the x value in Na_xMoS_2 is only x = 0.19. After this range, a voltage plateau starts with an average potential value of 1.39 V as can be observed in the first derivative of the galvanostatic curve (SI Figure S9). This plateau is related to the insertion reaction of Na into MoS_2 that undergoes a second order phase transition from molybdenite (2H−MoS_2) to Na_xMoS_2 for 0.5 < x < 1.0 (x < 2 for monolayer chalcogenide).[14,17] Throughout this range, the EPR signal intensity continues to slowly decrease up to 1.0 V, approximately ($x \approx 0.75$). The decrease in intensity, up to 77.1%, can be described as arising from the aforementioned process for few-layer MoS_2. Indeed, the fact that the signal intensity decreases weakly after 1.0 V vs Na/Na$^+$, reveals the relationship between the initial strong decrease in intensity and the higher conductivity of the composite reflected in the Dysonian line shape (Figure S8A), which can be attributed to the lower quantity of restacking faults and the synergic effect of the carbon nanotubes. The calculated asymmetry degree (A/B) of the Dysonian line shape upon discharging can be observed in Figure S10. It shows nearly constant values of ∼2.1 until a strong increase below 1.5 V vs Na/Na$^+$. The increase grows faster after 1.0 V vs Na/Na$^+$ finding a maximum value of ∼3.2 for 0.5 V vs Na/Na$^+$ and, then, decreasing to ∼2.5 at the cutoff potential value. This effect can be attributed to changes in the conductivity of the probed spins (σ_{spin}) upon sodium insertion, since both parameters are proportional (A/B $\propto \sigma_{spin}$).[58,59] This is in good agreement with the fact that valence electrons from the intercalant atoms are donated to the MoS_2, the transition to the metallic trigonal 1T phase and the final distortion and exfoliation that occurs when further Na incorporation (eq 2) takes place through a conversion reaction mechanism (solid state Na diffusion more likely than Na adsorption) so that Na_2S and Mo are formed.[40,55] In fact, Dysonian lines only appear when the sample thickness is fairly approximated or greater than the skin depth δ.[60] The skin depth can be defined as the distance between the particle surface and an inner point where the eddy currents reach a value of I_0/e (where I_0 is the surface current density and e is Euler's number), and it is at this depth where the electrons are expected to be the origin of the signal. Hence, the given contribution from the conduction electron paramagnetic resonance (CEPR) signal can be derived from changes in the composite line shape. There is an evident loss in signal intensity (Figure 4D), when the potential reaches around 0.2 V that can be attributed to a decrease in the density of spins derived from the final reduction of molybdenum centers at very low potential and the SEI formation. When the curve reaches the cutoff potential of 0.05 V vs Na/Na$^+$, the x value was 3.14 and therefore the discharge capacity was around 525 mAh g^{-1}.

With regard to the signal at g = ∼1.95, Figure 4A,B shows that it does not follow a clear trend. However, its weak intensity makes it difficult to infer many other details from the line shape. Despite the fact that its weakness makes the line shape ill-defined, the g value allows us to tentatively assign this resonance to either originating from stacking faults with a diminished quantity compared to that of the pure MoS_2 due to the synergic effect of the added carbon nanotubes, or arising from a small amount of hydrated pentacoordinated Mo^{5+} due to the closeness of the perpendicular g component to that previously reported in the literature.[61]

The galvanostatic curve upon charge (Figure 4E) does not show any extended plateau. However, in the potential range 1.5−2.0 V, the curve describes a pseudoplateau that has been previously related to the extraction of sodium atoms from the host material. Prior to this pseudoplateau, Mo and Na_2S formed in the conversion reaction during discharge (eq 2) has been partially converted, and reformation of MoS_2 takes place.[17,62]

DOI: 10.1021/acs.chemmater.7b01245
Chem. Mater. 2017, 29, 5886−5895

The in operando EPR spectra of the signal at g = 2.001, upon charging of the cell, shows a very slight decrease in intensity up to 1.2 V, and then, an increase that continues at an almost constant rate between 1.5 V and around 2.2 V. The poorly reversible initial reformation of Mo(0) and Na_2S into MoS_2 can be related to the slight decrease in intensity, whereas the subsequent increase in intensity can be related to the pseudoplateau observed in Figure 4E, where the main extraction reaction takes place, and then, molybdenum starts undergoing reoxidation toward Mo^{5+}.

Between 2.0 V and around 2.5 V the value of intensity stays nearly constant and increases, again, very strongly in the range 2.5 to 2.75 V vs Na/Na^+, whereas the asymmetry degree (Figure S8) decreases suddenly at around 2.25 V, and slowly decreases in the range 2.5 to 2.75 V. Given that the asymmetry degree is proportional to the conductivity of the probe electrons and the intensity proportional to the number of spins, this behavior can be interpreted as being related to the final stage in the formation of the MoS_2 small particles most probably with a higher degree of amorphousness, extra exfoliation, and/or increased interlayer space where Mo^{5+} defects can be more easily, reversibly, produced. Therefore, apart from the aforementioned synergic effects, the increase in the effective grain size can be directly connected to the better conductivity in the composite promoted by the highly conductive electrical links between few-layer MoS_2 particles created by CNTs acting as "bridges", which supports the improved reversibility of the electrochemical processes that take place upon sodiation and desodiation. The electrochemical properties of the composite are further studied in the SI 9 (Figures S11 and S12).

Summarizing, the analysis from EPR, while discharging, identically to the in operando for the pure Ex-MoS_2 (Figures S5 and S6), the signal intensity of the of the signal centered at g = 2.001 decreases upon sodiation and no other signal arises during discharge, but interestingly, the signal was recovered during the charging stage, even though the cutoff potential was 0.05 V vs Na/Na^+, giving rise to a reversible process. The electrochemical processes that occur can be related to the increase in the degree of asymmetry (A/B) of the Dysonian line shape while decreasing in signal intensity upon sodiation, and the opposite behavior occurs upon desodiation.

In order to assess the further reversible sodiation of the subsequent cycles, an in operando EPR measurement was carried out during the first cycles of the composite material. The electrochemical test consisted of a cyclic voltammetry (CV) carried out at 0.05 mV s^{-1} to control the potential variation while the current response and EPR spectra were recorded. In Figure 5, the evolution of the spectra can be seen as well as the cyclic voltammograms and the obtained normalized intensity for the resonances as a function of potential.

The 0 V spectra displayed a resonance at g = 2.007 that can be attributed to the aforementioned S-Mo^{5+} defects. There was no clear signal at g = 1.954, which reflects some sample variability. The resonances on monitoring of the spectra while varying the potential showed behavior very similar to that previously observed during the galvanostatic cycling, although did not present as intense degree of asymmetry. This lower asymmetry degree can be explained as a result of the lower current implied in the electrochemical processes since the potential is now the fixed parameter unlike during the galvanostatic cycling where a higher current was the constant

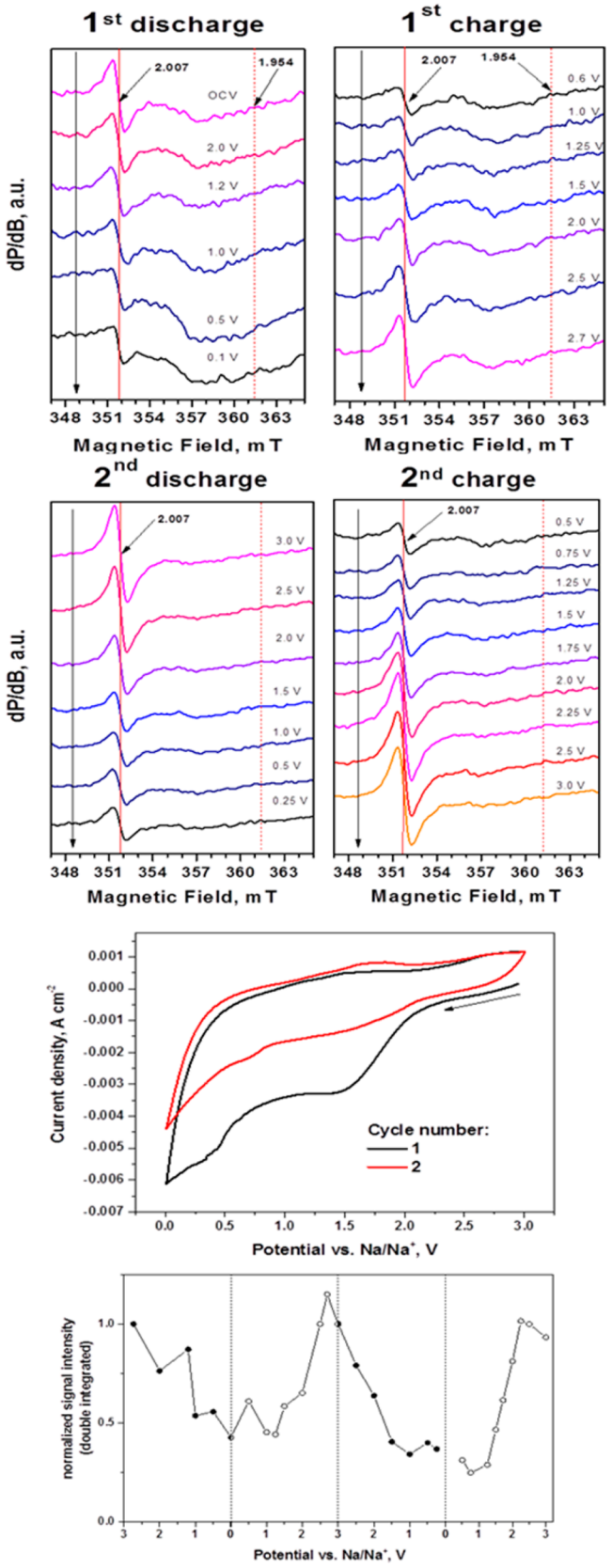

Figure 5. In operando EPR spectra of the Ex-MoS_2/CNTs composite vs Na of the 1st and 2nd cycles (top plots). Cyclic voltammograms of the 1st (black line) and 2nd (red line) cycles (middle plot) and plot of the normalized EPR intensity of the resonances at different voltage values for charge and discharge (bottom plot).

DOI: 10.1021/acs.chemmater.7b01245
Chem. Mater. 2017, 29, 5886−5895

parameter. It can be inferred from the in operando data of Figure 5 that there is a reversible trend in the variation of the signal intensity of the observed resonance which decreases upon sodium intercalation and increases upon sodium extraction. The fact that this trend was not constant for the whole potential range suggests that the Na^+ adsorption on the related defects was potential dependent and its gradient was higher for the range around 3.0 V to 1.0 V vs. Na/Na^+ whereas in the range around 1.0 V to 0.05 V vs. Na/Na^+ it was nearly constant. This was consistent with the previously observed trend in the galvanostatic experiment and the above explanation. Upon the first discharge (Figure 5), the signal intensity (proportional to density of spins) decreased below 45% of the initial value and was totally recovered when the potential value reached the original open circuit potential (OCP) and was further increased when the CV oxidative branch went further up to 3.0 V. This suggests that the oxidative potential creates defects responsible for the EPR signal at a concentration higher than the initial amount.

Furthermore, it can be observed for the second discharge that the final value of signal intensity was even lower than the first discharge (by around 36%) even though the starting intensity value was higher. This implies that the defect's creation/neutralization mechanism was not related to the reversible capacity loss but, on the contrary, related to the increase in charge capacity during the first cycles.

CONCLUSIONS

We have developed a cell that allows use for in operando EPR electrochemical measurements. The results for few-layer MoS_2 suggest that the mechanism of sodiation is established by first decreasing the density of Mo^{5+} defects at low symmetry sites, and even though the obtained specific capacity is higher than that of the multilayer chalcogenide, this process shows low reversibility for this material. The composite of few-layer MoS_2 and single walled carbon nanotubes shows reversible behavior due to the enhanced conductivity and synergic effects produced between the carbonaceous material and the few-layer chalcogenide. The achieved stark electronic linking between nanoparticles allows a good cycling stability even at low cutoff potential, improving the obtained specific capacity and energy density. The composite shows reversible EPR spectra where high conductivity electrons related to the Mo^{5+} paramagnetic centers can be observed, which may be responsible for the fast adsorption mechanism. Moreover, the reversible EPR spectra implies the adsorption and desorption of Na^+ ions on the Mo^{5+} defects or their neutralization during the sodiation process and subsequent creation upon extraction.

Further development of in operando electrochemical EPR will help us to understand more deeply many of the complex issues regarding electrochemical energy storage, allowing reach of the higher capacities demanded by today and future society.

ASSOCIATED CONTENT

Supporting Information

The Supporting Information is available free of charge on the ACS Publications website at DOI: 10.1021/acs.chemmater.7b01245.

34 GHz EPR measurements; EPR spectral details of CNTs; Time dependent EPR measurements; Galvanostatic curves of few-layer MoS_2; in operando EPR measurements for few-layer MoS_2; XRD data; Dysonian line simulation; galvanostatic derivative of few-layer MoS_2/CNTs composite cycling; asymmetry degree as a function of potential; further study of the electrochemical properties of the composite few-layer MoS_2/CNTs; results of variation of the potential window; in operando EPR measurements for multilayer MoS_2/CNTs; XPS results for the few-layer MoS_2/CNTs composite; and morphological characterization of few-layer MoS_2/CNTs (PDF)

AUTHOR INFORMATION

Corresponding Authors

*E-mail: jose.gonzalezjimenez@manchester.ac.uk (J.R.G.).
*E-mail: alistair.fielding@manchester.ac.uk (A.J.F.).
*E-mail: robert.dryfe@manchester.ac.uk (R.A.W.D.).

ORCID

José L. Tirado: 0000-0002-8317-2726
Alistair J. Fielding: 0000-0002-4437-9791
Robert A. W. Dryfe: 0000-0002-9335-4451

Author Contributions

All authors have given approval to the final version of the manuscript.

Notes

The authors declare no competing financial interest.

ACKNOWLEDGMENTS

We would like to thank the European Union Seventh Framework Programme under grant agreement no. 604391 Graphene Flagship, MINECO (MAT2011-22753, EEBB-I-16-10801), EPSRC (grant ref. EP/K016954/1), the EPSRC National Electron Paramagnetic Resonance service at The University of Manchester, Ben Spencer for acquiring the XPS data and Professor David Collison for critically reading the manuscript.

REFERENCES

(1) Tarascon, J. M.; Armand, M. Issues and Challenges Facing Rechargeable Lithium Batteries. *Nature* **2001**, *414*, 359−367.
(2) Yaksic, A.; Tilton, J. E. Using the Cumulative Availabiity Curve To Assess. *Resour. Policy* **2009**, *34*, 185−194.
(3) Palomares, V.; Serras, P.; Villaluenga, I.; Hueso, K. B.; Carretero-González, J.; Rojo, T. Na-Ion Batteries, Recent Advances and Present Challenges to Become Low Cost Energy Storage Systems. *Energy Environ. Sci.* **2012**, *5*, 5884−5901.
(4) Ellis, B. L.; Nazar, L. F. Sodium and Sodium-Ion Energy Storage Batteries. *Curr. Opin. Solid State Mater. Sci.* **2012**, *16*, 168−177.
(5) Hong, S. Y.; Kim, Y.; Park, Y.; Choi, A.; Choi, N.-S.; Lee, K. T. Charge Carriers in Rechargeable Batteries: Na Ions vs. Li Ions. *Energy Environ. Sci.* **2013**, *6*, 2067−2081.
(6) Chevrier, V. L.; Ceder, G. Challenges for Na-Ion Negative Electrodes. *J. Electrochem. Soc.* **2011**, *158*, A1011.
(7) Wang, Q.; Ping, P.; Zhao, X.; Chu, G.; Sun, J.; Chen, C. Thermal Runaway Caused Fire and Explosion of Lithium Ion Battery. *J. Power Sources* **2012**, *208*, 210−224.
(8) Lisbona, D.; Snee, T. A Review of Hazards Associated with Primary Lithium and Lithium-Ion Batteries. *Process Saf. Environ. Prot.* **2011**, *89*, 434−442.
(9) Miki, Y.; Nakazato, D.; Ikuta, H.; Uchida, T.; Wakihara, M. Amorphous MoS2 as the Cathode of Lithium Secondary Batteries. *J. Power Sources* **1995**, *54*, 508−510.
(10) Sen, U. K.; Mitra, S. High-Rate and High-Energy-Density Lithium-Ion Battery Anode Containing 2D MoS2 Nanowall and Cellulose Binder. *ACS Appl. Mater. Interfaces* **2013**, *5*, 1240−1247.

DOI: 10.1021/acs.chemmater.7b01245
Chem. Mater. 2017, 29, 5886−5895

(11) Hwang, H.; Kim, H.; Cho, J. MoS2 Nanoplates Consisting of Disordered Graphene-like Layers for High Rate Lithium Battery Anode Materials. *Nano Lett.* **2011**, *11*, 4826−4830.
(12) Xiao, J.; Choi, D.; Cosimbescu, L.; Koech, P.; Liu, J.; Lemmon, J. P. Exfoliated MoS2 Nanocomposite as an Anode Material for Lithium Ion Batteries. *Chem. Mater.* **2010**, *22*, 4522−4524.
(13) Chang, K.; Chen, W.; Ma, L.; Li, H.; Li, H.; Huang, F.; Xu, Z.; Zhang, Q.; Lee, J.-Y. Graphene-like MoS2/amorphous Carbon Composites with High Capacity and Excellent Stability as Anode Materials for Lithium Ion Batteries. *J. Mater. Chem.* **2011**, *21*, 6251.
(14) Park, J.; Kim, J. S.; Park, J. W.; Nam, T. H.; Kim, K. W.; Ahn, J. H.; Wang, G.; Ahn, H. J. Discharge Mechanism of MoS2 for Sodium Ion Battery: Electrochemical Measurements and Characterization. *Electrochim. Acta* **2013**, *92*, 427−432.
(15) Wang, X.; Shen, X.; Wang, Z.; Yu, R.; Chen, L. Atomic-Scale Clarification of Structural Transition of MoS2 upon Sodium Intercalation. *ACS Nano* **2014**, *8*, 11394−11400.
(16) Wang, J.; Luo, C.; Gao, T.; Langrock, A.; Mignerey, A. C.; Wang, C. An Advanced MoS2/carbon Anode for High-Performance Sodium-Ion Batteries. *Small* **2015**, *11*, 473−481.
(17) David, L.; Bhandavat, R.; Singh, G. MoS2/Graphene Composite Paper For Sodium-Ion Battery Electrodes. *ACS Nano* **2014**, *8*, 1759−1770.
(18) Xie, X.; Ao, Z.; Su, D.; Zhang, J.; Wang, G. MoS2/graphene Composite Anodes with Enhanced Performance for Sodium-Ion Batteries: The Role of the Two-Dimensional Heterointerface. *Adv. Funct. Mater.* **2015**, *25*, 1393−1403.
(19) Kumar, P. R.; Jung, Y. H.; Kim, D. K. High Performance of MoS2Microflowers with a Water-Based Binder as an Anode for Na-Ion Batteries. *RSC Adv.* **2015**, *5*, 79845−79851.
(20) Raccichini, R.; Varzi, A.; Chakravadhanula, V. S. K.; Kübel, C.; Passerini, S. Boosting the Power Performance of Multilayer Graphene as Lithium-Ion Battery Anode via Unconventional Doping with in-Situ Formed Fe Nanoparticles. *Sci. Rep.* **2016**, *6*, 23585.
(21) Murphy, D. M. *EPR (Electron Paramagnetic Resonance) Spectroscopy of Polycrystalline Oxide Systems*; 2009; Vol. *1*.
(22) Eaton, G. R.; Eaton, S. S.; Barr, D. P.; Weber, R. T. *Quantitative EPR: A Practitioners Guide*; 2010.
(23) Weil, J.; Bolton, J. *Electron Paramagnetic Resonance: Elementary Theory and Practical Applications*; 2007.
(24) Lund, A.; Rhodes, C. J. *Radicals on Surfaces*; Lund, A., Rhodes, C. J., Eds.; Springer Science+Business Media, B.V.: Harvard, U.S.A., 1995.
(25) Silbernagel, B. G. Electron Spin Resonance of Sulfide Catalysts. *J. Magn. Magn. Mater.* **1983**, *31*−*34*, 885−886.
(26) Panich, M.; Shames, I.; Rosentsveig, R.; Tenne, R. A Magnetic Resonance Study of MoS(2) Fullerene-like Nanoparticles. *J. Phys.: Condens. Matter* **2009**, *21*, 395301.
(27) Deroide, B.; Bensimon, Y.; Belougne, P.; Zanchetta, J. V. Lineshapes of ESR Signals and the Nature of Paramagnetic Species in Amorphous Molybdenum Sulfides. *J. Phys. Chem. Solids* **1991**, *52*, 853−857.
(28) Young, C. G.; Collison, D.; Mabbs, F. E.; Enemark, J. H. The First Mononuclear molybdenum(V) Complex with a Terminal Sulfido Ligand: [HB(Me2C3N2H)3]MoSCl2. *Inorg. Chem.* **1987**, *26*, 2925−2927.
(29) Hill, J. P.; Laughlin, L. J.; Gable, R. W.; Young, C. G. *Inorg. Chem.* **1996**, *35*, 3447 10.1021/ic951645g
(30) Webster, R. D.; Dryfe, R. A. W.; Coles, B. A.; Compton, R. G. In Situ Electrochemical EPR Studies of Charge Transfer across the Liquid/Liquid Interface. *Anal. Chem.* **1998**, *70*, 792−800.
(31) Compton, R. G.; Waller, A. M. ESR Spectroscopy of Electrode Processes. In *Spectroelectrochemistry: Theory and Practice*; Gale, R. J., Ed.; Springer US: Boston, MA, 1988; pp 349−398.
(32) Lamy, C.; Crouigneau, P. In Situ Electron Spin Resonance Spectroscopy Studies of Electrode Processes. *J. Electroanal. Chem. Interfacial Electrochem.* **1983**, *150*, 545−552.
(33) Tamski, M. A.; Macpherson, J. V.; Unwin, P. R.; Newton, M. E. Electrochemical Electron Paramagnetic Resonance Utilizing Loop Gap Resonators and Micro-Electrochemical Cells. *Phys. Chem. Chem. Phys.* **2015**, *17*, 23438−23447.
(34) Sathiya, M.; Leriche, J.-B.; Salager, E.; Gourier, D.; Tarascon, J.-M.; Vezin, H. Electron Paramagnetic Resonance Imaging for Real-Time Monitoring of Li-Ion Batteries. *Nat. Commun.* **2015**, *6*, 6276.
(35) Coleman, J. N.; Lotya, M.; O'Neill, A.; Bergin, S. D.; King, P. J.; Khan, U.; Young, K.; Gaucher, A.; De, S.; Smith, R. J.; et al. Two-Dimensional Nanosheets Produced by Liquid Exfoliation of Layered Materials. *Science (Washington, DC, U. S.)* **2011**, *331*, 568−571.
(36) Bissett, M. A.; Kinloch, I. A.; Dryfe, R. A. W. Characterization of MoS 2 − Graphene Composites for High-Performance Coin Cell Supercapacitors. *ACS Appl. Mater. Interfaces* **2015**, *7*, 17388−17398.
(37) Novoselov, K. S.; Mishchenko, A.; Carvalho, A.; Neto, A. H. C.; Road, O. 2D Materials and van Der Waals Heterostructures. *Science* **2016**, *353*, 461.
(38) Bensimon, Y.; Belougne, P.; Giuntini, J.; Zanchetta, J. V. Electron Spin Resonance of Water Adsorption on Amorphous Molybdenum Sulfide. *J. Phys. Chem.* **1984**, *88*, 2754−2757.
(39) Bensimon, Y.; Belougne, P.; Deroide, B.; Zanchetta, J. V.; Giuntini, J. C.; Henn, F. ESR Study of Influence of Oxygen on Molybdenum Sulfides. *J. Non-Cryst. Solids* **1992**, *149*, 218−228.
(40) Arčon, D.; Zorko, A.; Cevc, P.; Mrzel, A.; Remškar, M.; Dominko, R.; Gaberšček, M.; Mihailović, D. Electron Spin Resonance of Doped Chalcogenide Nanotubes. *Phys. Rev. B: Condens. Matter Mater. Phys.* **2003**, *67*, 1−10.
(41) Seifert, G.; Terrones, H.; Terrones, M.; Jungnickel, G.; Frauenheim, T. Structure and Electronic Properties of MoS2 Nanotubes. *Phys. Rev. Lett.* **2000**, *85*, 146−149.
(42) Blinc, R.; Cevc, P.; Mrzel, A.; ArcOn, D.; Remškar, M.; Milia, F.; Laguta, V. V. EPR Spectra of MoS2/C60. *Phys. Status Solidi B* **2010**, *247*, 3033−3034.
(43) Cai, L.; He, J.; Liu, Q.; Yao, T.; Chen, L.; Yan, W.; Hu, F.; Jiang, Y.; Zhao, Y.; Hu, T.; et al. Vacancy-Induced Ferromagnetism of MoS_2 Nanosheets. *J. Am. Chem. Soc.* **2015**, *137*, 2622−2627.
(44) Sobczynski, A.; Zmierczak, W. Characterization of MoS2/SiO2 by ESR and NO Adsorption. *React. Kinet. Catal. Lett.* **1991**, *44*, 511−516.
(45) Averill, B. A.; Orme-Johnson, W. H. Electron Paramagnetic Resonance Spectra of Molybdenum(III) Complexes: Direct Observation of 95Mo Hyperfine Interaction and Implications for Molybdoenzymes. *Inorg. Chem.* **1980**, *19*, 1702−1705.
(46) Julien, C.; Mauger, A.; Vijh, A.; Zaghib, K. *Lithium Batteries*; Springer International Publishing Switzerland: New York, 2016.
(47) Park, M. S.; Needham, S. A.; Wang, G. X.; Kang, Y. M.; Park, J. S.; Dou, S. X.; Liu, H. K. Nanostructured SnSb/carbon Nanotube Composites Synthesized by Reductive Precipitation for Lithium-Ion Batteries. *Chem. Mater.* **2007**, *19*, 2406−2410.
(48) Petit, P.; Jouguelet, E.; Fischer, J. E.; Rinzler, A. G.; Smalley, R. E. Electron Spin Resonance and Microwave Resistivity of Single-Wall Carbon Nanotubes. *Phys. Rev. B: Condens. Matter Mater. Phys.* **1997**, *56*, 9275−9278.
(49) Adhikari, A.; Bakhru, H.; Ajayan, P.; Benson, R.; Chipara, M. Electron Spin Resonance Investigations on Ion Beam Irradiated Single-Wall Carbon Nanotubes. *Nucl. Instrum. Methods Phys. Res., Sect. B* **2007**, *265*, 347−351.
(50) Abraham, D. P.; Shkrob, I. A.; Zhu, Y.; Marin, T. W.; Abraham, D. Reduction of Carbonate Electrolytes and the Formation of Solid-Electrolyte Interface (SEI) in Lithium-Ion Batteries. 1. Spectroscopic Observations of Radical Intermediates Generated in One-Electron Reduction of Carbonates. *J. Phys. Chem. C* **2013**, *117*, 19255−19269.
(51) Adem, E.; Burillo, G.; Munoz, E.; Rickards, J.; Cota, L.; Avalos-borja, M. Electron and Proton Irradiation of Poly(vinylidene Fluoride): Characterization by Electron Paramagnetic Resonance. *Polym. Degrad. Stab.* **2003**, *81*, 75−79.
(52) Tiwari, V. K.; Rath, M. C.; Sarkar, S. K.; Patel, V. K.; Ray, B.; Maiti, B.; Maiti, P. Electron Beam-Induced Piezoelectric Phase in Poly(vinylidene Fluoride) Nanohybrid: Effect at the Molecular Level. *Polym. Int.* **2015**, *64*, 212.

DOI: 10.1021/acs.chemmater.7b01245
Chem. Mater. 2017, 29, 5886−5895

(53) Mortazavi, M.; Wang, C.; Deng, J.; Shenoy, V. B.; Medhekar, N. V. Ab Initio Characterization of Layered MoS2 as Anode for Sodium-Ion Batteries. *J. Power Sources* **2014**, *268*, 279−286.
(54) Ahmed, B.; Anjum, D. H.; Hedhili, M. N.; Alshareef, H. N. Mechanistic Insight into the Stability of HfO2-Coated MoS2 Nanosheet Anodes for Sodium Ion Batteries. *Small* **2015**, *11*, 4341−4350.
(55) Su, J.; Pei, Y.; Yang, Z.; Wang, X. Ab Initio Study of Graphene-like Monolayer Molybdenum Disulfide as a Promising Anode Material for Rechargeable Sodium Ion Batteries. *RSC Adv.* **2014**, *4*, 43183−43188.
(56) Wang, X.; Shen, X.; Wang, Z.; Yu, R.; Chen, L. Atomic-Scale Clarification of Structural Transition of MoS2 upon Sodium Intercalation. *ACS Nano* **2014**, *8*, 11394−11400.
(57) Tadyszak, K.; Strzelczyk, R.; Coy, E.; Mac'Kowiak, M.; Augustyniak-Jabłokow, M. A. Size Effects in the Conduction Electron Spin Resonance of Anthracite and Higher Anthraxolite. *Magn. Reson. Chem.* **2016**, *54*, 239−245.
(58) Sitaram, V.; Sharma, A.; Bhat, S. V.; Mizoguchi, K.; Menon, R. Electron Spin Resonance Studies in the Doped Polyaniline PANI-AMPSA: Evidence for Local Ordering from Linewidth Features. *Phys. Rev. B: Condens. Matter Mater. Phys.* **2005**, *72*, 35209.
(59) Rice, W. D.; Weber, R. T.; Nikolaev, P.; Arepalli, S.; Berka, V.; Tsai, A.-L.; Kono, J. Spin Relaxation Times of Single-Wall Carbon Nanotubes. *Phys. Rev. B: Condens. Matter Mater. Phys.* **2013**, *88*, 41401.
(60) Takizawa, T.; Nomura, S.; Goltzen, A.; Schwab, C. Dysonian Line in the Electron Spin Resonance of Highly Conductive CuIn2S4 Single Crystals. *Jpn. J. Appl. Phys.* **1993**, *32*, 479−480.
(61) Louis, C.; Che, M. EPR Investigation of the Coordination Sphere of Mo5 + Ions on Thermally Reduced Silica-Supported Molybdenum Catalysts Prepared by the Grafting Method. *J. Phys. Chem.* **1987**, *91*, 2875−2883.
(62) Sahu, T. S.; Mitra, S. Exfoliated MoS2 Sheets and Reduced Graphene Oxide-An Excellent and Fast Anode for Sodium-Ion Battery. *Sci. Rep.* **2015**, *5*, 12571.

■ NOTE ADDED AFTER ASAP PUBLICATION

This article was published ASAP on July 17, 2017, with incorrect versions of Figures 1 and 2. The corrected article was published ASAP on July 25, 2017.

DOI: 10.1021/acs.chemmater.7b01245
Chem. Mater. 2017, 29, 5886−5895